Technique for Low Amperage Potline Operation for Electricity Grid Storage

MARK P. TAYLOR and JOHN J.J. CHEN

Following a critical review and analysis of steady-state energy balance windows for large modern cell technologies [*Taylor* et al., *Met. Mat. Transactions E, 9th Sept. 2014*], the issue of a substantial reduction in energy input and heat output to a specific cell technology is addressed in this paper. To investigate the feasibility of such a reduction, the dynamic response to substantial changes in cell amperage and energy input must be quantified. If large amperage reductions can be shown to be feasible and to have no major detrimental affects, a flexible amperage operating philosophy would allow the use of smelting cells as an energy reservoir in the following way: in times of high electricity demand the cells would operate at reduced amperage, releasing electricity to the grid, while in times of low demand or an over-supply of electricity on the grid, the cells would store the surplus electricity in the form of additional aluminum metal. However, to take the above concept out of the realms of the theoretical, it will first be necessary to demonstrate an ability to predict and control the response of the cell to such changes in energy input through regulating the heat losses from the cell. The process of regulation of cell heat loss is quite foreign to operators of aluminum smelters, because the technology to regulate heat loss from smelting cells has not existed previously. This technology does now exist in the form of patented heat exchangers [*Taylor* et al., *US Patent 7,901,617 B2, Mar. 8, 2011*], but its impact on smelter cell walls must be examined in a dynamic analysis to determine the effect on the molten bath temperature and liquid mass within the cell. The objective of this paper therefore is to perform a first-order analysis of this problem, and to identify the key scientific issues in regulating cell heat loss and in the operating philosophy of heat loss regulation.

DOI: 10.1007/s40553-015-0046-9

I. INTRODUCTION

GLOBALLY, the nature of electricity demand has been impacted by two key factors in the past few decades; firstly, the increasing interconnection of larger and larger urban centers, and even countries (as in Europe), magnifying both the diurnal, weekly, and seasonal MW demand curves, as well as bringing about greater risk of large scale supply problems through network failure (*e.g.*, North Eastern USA and Canada, 2003, and again in 2008). The second trend is toward greater renewable energy generation in developed nation networks, with wind power in Germany making up more than 20 pct of all generation from 2013. Renewable generation has increased both the variability of electricity supply, and also increased the gap between supply required and the total generating capacity.

The net result of the above trends is that there are severe supply and price volatilities in the electricity market, and that there are many periods when expensive generating capacity is not used, or is wasted—as is the case when hydro-electric storage must be spilled due to lack of sufficient demand or storage. Aluminum smelters cannot currently participate in demand-side regulation because there is no significant turn up or turndown capacity in these production units, other than turning them off altogether, or building new ones. If a smelter's power usage of 500 to 1000 MW could be used flexibly, with turn up/turndown of 30 to 40 pct each, countries or electricity networks with existing smelting capacity could utilize all efficient generating capacity, and potential shortages could be reduced or eliminated. The economic value of these outcomes for countries or electricity networks is very significant.

Furthermore, the aluminum produced during periods of surplus generation can be viewed as stored electricity, and may be used to generate transport fuels such as hydrogen[1] to complete an integrated energy supply network for a country or a community.

In contrast to the above vision of flexibility, present smelter turn up and turndown is in the range ± 5 pct for a smelter using 300 to 400 kA potline technologies. The fundamental constraints in smelting cell energy balance are discussed in detail in a previous paper.[2] The outstanding issue which remains un-addressed in the literature, and in the industry is that approximately 85 pct of the heat loss from aluminum smelting cells is driven by the superheat and volume of the bath (and metal), and cannot be regulated independently of these key characteristics. Therefore, it is currently not possible

MARK P. TAYLOR, Professor, Department of Chemical and Materials Engineering, University of Auckland, Private Bag 92019, Auckland 1142, New Zealand, and also Director with the NZ Product Accelerator, University of Auckland, Private Bag 92019, Auckland 1142, New Zealand. Contact e-mail: mark.taylor@auckland.ac.nz JOHN J.J. CHEN, Professor, is with the Department of Chemical and Materials Engineering, University of Auckland.

Manuscript submitted October 11, 2014.
Article published online February 21, 2015

to alter heat dissipation significantly to allow flexible power input and amperage, without unacceptable changes in bath superheat and volume.

A product of this constraint is that industry efforts to modulate potline amperage, and through this smelter power usage, have been fraught with difficulty over the past 30 to 40 years, despite sound economic drivers and periodic imperatives to quickly reduce smelter power usage.[3]

In almost all cases of modulation or regular smelter power reductions, decreases in amperage have been in the range from 5 to 20 kA. Even with decreases of this magnitude (5 to 10 pct amperage reduction or less), the cumulative effect of the heat balance fluctuations over months became performance limiting and probably unsustainable, especially if these modulations occurred with any regularity—for example, Valesul[4] and Aldel[5] both implemented modulation of varying magnitudes but neither found the process sustainable in the long term. Cathode performance, cell instability, and current efficiency were variously degraded in at least a proportion of the cells in these smelters and the modulation processes were discontinued.

The largest sustained smelter power reductions have been those forced on Hillside and Mosal smelters in Africa, due to a mandatory electricity supply reduction of 10 pct in 2008 by the utility Eskom Holdings. Between 20 and 25 kA potline amperage, reductions were necessary at these latter smelters, and were made possible by turning off the air blowing manifolds which previously cooled the whole of the potshell of each pot. These blowers had dissipated more heat, allowing the pots to reach higher amperages of 370 to 380 kA. Even so, only a limited sustainable reduction in total smelter power was possible at these smelters,[6] due to no downward flexibility in cell heat losses.

A new technology for downward and upward cell heat loss control has been developed and is described fully in several US Patents[7,8] from 2011 and 2014. In steady-state experiments,[3] this technology has been demonstrated to insulate the walls of a smelting cell externally using its proprietary heat exchangers, in order to offset the effect of lower cell amperage and surplus heat generation in the bath. Controlled reduction of the cell duct draft complements the reduction in wall heat loss, in order to correct for the lower heat generation in the anodes and lower heat transmission through the crust.

Of necessity in a complex process like a smelting cell, this technology requires comprehensive industrial cell testing to understand the dynamics of the response of the cell to both a change in amperage and a change in cell wall and top heat losses designed to correct it. In this paper, we explore these dynamics using a simple computational approach to expose the underlying questions and potential problems with such an approach to smelter operation.

The scientific question can be summarized as follows: *how does a smelting cell react to large changes in the heat generation (through reduced amperage in this case), under reduced heat loss conditions ?*

The first issue in terms of the validity of the flexible technology direction must be: *how much heat loss reduction is actually needed to stabilize the energy balance after such a change in amperage ?*

The intent of the present paper is exploratory to confirm the validity of the heat loss regulation concept. We are aiming to understand if the technology concept can stabilize the overall energy balance. If so what extent of heat loss regulation is required in order to do this, and what critical control parameters and interactions exist ?

II. METHODOLOGY

A. *A Hypothetic Case Study*

In order to manage the power cost for a smelter, the following information exists about the cells at this smelter:

- 3 lines of 280 cells each.
- Cell voltage = 4.0 V, including a bus bar voltage drop totalling 0.2 V external to the cell.
- Cell amperage = 240 kA.
- Current efficiency = 94 pct.
- Sidewall heat loss = 38 pct of total heat dissipation, and the internal sidewall area is 4 m × 9 m × 0.5 m high.
- Total internal ohmic voltage at 240 kA = 2.1 V.
- Average bath temperature is 1233 K (960 °C) and average liquidus temperature is 1223 K (950 °C).
- Average XS AlF_3 pct is 10 pct and bath mass is 4500 kg.
- One centimeter of bath height (1 cm) = 200 kg of liquid bath mass, in this cell technology.

Some fundamental data about the bath and the electrochemical voltage breakdown are available.[9]

Wall heat transfer coefficient from bath/metal to ledge, h	800 W/m^2 °C
C_p bath	1.7 kJ/kg °C
ΔH fusion	520 kJ/kg
Decomposition potential	1.20 V
Overpotential (anode and cathode)	0.50 V
Theoretical energy to make AL at 94 pct CE	6.5 kWh/kg

A proposal from the smelter's power supplier is for the smelter to reduce current from 240 to 160 kA (300 to 350 MW flexibility required by the power supplier) on an irregular basis when domestic power usage in the neighboring city is high. This could be for a few hours or even a few months, and no definitive time scale for the duration or frequency of reductions is available from the power supplier.

This proposal is going to be difficult to implement, but the alternative may be that the total power block for the smelter is reduced substantially at the coming power renegotiations. Therefore, the Plant Manager has decided to check the viability of an 80 kA reduction in amperage and to seek ways to mitigate the effects of these reduced amperage events, should they be required.

In addressing this question, it is essential first to determine the energy imbalance which would

instantaneously occur through this current reduction, assuming initially that the anode–cathode distance, or ACD is not changed when the current reduction occurs, because significant ACD changes cause top crust deterioration and reduce bath height rapidly.

Ultimately, the answer to the Plant Manager's question centers on how long such an energy imbalance is able to be sustained on these cells, before the bath temperature is reduced below a critical value for operating the smelting process, and in particular for dissolving alumina. For conventional smelting baths, this critical temperature is assessed here to be 1173 K (900 °C), or slightly above, for the following reasons: at temperatures (and liquidus temperatures) below 1173 K (900 °C) the composition of the liquid is essentially chiolitic as shown in the NaF-AlF_3 phase diagram, with less than 5 pct of cryolite remaining. This causes the alumina concentration in the bath to become too low to prevent anode effect, because in addition to the low temperature, the saturation solubility of the alumina is reduced below 5 wt pct, as noted recently by Cassayre *et al.*[10] Therefore, the alumina dissolution process becomes mass transfer limited as well as heat transfer constrained, and the electrolysis process becomes infeasible at industrial current densities due to almost constant anode effects, which would occur on many cells in a potline subjected to the same low-temperature conditions.

The second, related question to be addressed in this work is: what degree of heat loss regulation, or '*Flexible Production Technology'* would be sufficient to make this scenario feasible for the smelter on an ongoing basis? A simple lumped heat capacity computation is derived below to explore this question, prior to industrial experimentation.

B. *Development of Simplified Energy Balance for the Cell With, and Without Heat Exchangers and Reduced Duct Draft*

1. *Thermodynamic basis*

At the original amperage of 240 kA, the electrochemical voltage breakdown of the cell is as follows (as given in Section II–A):

$$\begin{aligned} V &= 1.7(\text{decomposition potential and overvoltage}) \\ &\quad + 2.1(\text{cell ohmics}) + 0.2(\text{external bus bar}) \\ &= 4.0\text{V} \end{aligned}$$

The Ohmic resistance can be calculated as 2.1 V/240 kA = 8.75 micro-ohms, at the cell voltage supplied.

The energy available for heat dissipation depends on the energy used in the electrochemical reaction of alumina with carbon to produce aluminum

$$V_{\text{reaction}} = 2.05V\,(\text{from } 298 \times V/CE = 6.5\,\text{kWh/kg AL})$$

and these energy and voltage requirement do not change with amperage unless *CE*, the current efficiency changes as well.

Based on the above breakdown, the starting heat dissipation of the cell at full amperage is given by

$$\begin{aligned} Q_{\text{original}} &= (4.0{-}0.2{-}2.05) \times 240\,\text{kA} \\ &= 420\,\text{kW heat dissipation.} \end{aligned}$$

This is the steady-state heat loss of the cell at its original amperage.

From the previous thermo-electrical cell analyses,[2] a proportion of 38 pct of Q_{original} is exiting through the walls (side and end) of modern cells, and 48 pct *via* the top of the cell. These assumptions are discussed in the Section II–B below. Hence

$$\begin{aligned} Q_{\text{walls}} &= 0.38 \times 420\,\text{kW} = 159.6\,\text{kW} \\ Q_{\text{top}} &= 0.48 \times 420\,\text{kW} = 201.6\,\text{kW} \end{aligned}.$$

Now, at the reduced amperage of 160 kA, it is assumed that the electrochemically generated voltage does not change from the value of 1.7 V given above, although the anode activation polarization does depend weakly on the anode current density (Tafel, logarithmic dependence). However, a reduced bath temperature during the lower amperage operation will tend to increase both the decomposition potential (through the free energy change) of the cell reaction and the various components of anode and cathode polarization as well. These upward pressures on voltage will negate and possibly exceed the downward Tafel dependence of the anode activation polarization as bath temperature reduces.

The competing electrochemical effects are self-correcting because reduced bath temperatures in the anode—cathode space after the amperage decrease will trigger higher electrochemical voltage drops and more heat generation, with higher local temperatures. These dynamics are not addressed here but will be monitored through fast data acquisition of cell voltage and amperage during the industrial cell testing program. The case simulated here is a worst case in terms of the shock to the energy balance, since no extra heat generation is included from higher electrochemical voltage drop

$$\begin{aligned} V(\text{at } 160\,\text{kA}) &= 1.7V + 160\,\text{kA} \times 8.75\,\text{micro-ohms}/ \\ &\quad 1000 + 0.2V \times (160/240) \\ &= 3.235V. \end{aligned}$$

This value is the total cell voltage, and includes the external bus bar component. Removing this bus bar component gives the internal cell voltage

$$V(\text{internal cell}) = 3.101V,$$

compared with the full amperage situation which was 3.8 V. Now, the new heat dissipation inside the cell at 160 kA is

$$Q_{\text{e}} = (3.101{-}2.05) \times 160\,\text{kA} = 168.16\,\text{kW},$$

at this reduced amperage.

Therefore the Instantaneous Energy Imbalance
$= Q_{\text{original}} - Q_e = 420\,\text{kW} - 168.2\,\text{kW}$
$= 251.8\,\text{kW}, \quad \text{at } t = 0,$
immediately after the amperage reduction.

From this basis, in the following section, the major energy balance dynamics are formulated.

2. *Global energy imbalance*

The above calculations of instantaneous global energy imbalance can be summarized in the following way. First, the defining equation for the energy imbalance at time zero is

$$\Delta\text{Energy}_o = Q_{\text{original}} - Q_e = I_o \times (V_o - V_{\text{reaction}} - I_o \times R_{\text{ext}}) - I_e \times (V_e - V_{\text{reaction}} - I_e \times R_{\text{ext}}), \quad [1]$$

where Q_{original} is the steady-state cell heat dissipation, Q_e is the new heat dissipation available at the lower amperage, and the subscripts 'o' and 'e' refer to the original and reduced amperage situations, respectively. Equation [1] expresses this calculation of initial energy imbalance, resulting in a 251.8 kW imbalance, at the instant the amperage is reduced to 160 kA.

This imbalance equates to the rate of change of enthalpy of the cell

$$d(M \cdot C_p \cdot T)\text{cell}/\text{d}t = \Delta\text{Energy}_t, \quad [2]$$

the initial instantaneous energy imbalance at time t

Rapid thermal communication occurs between the bath, metal, cathode, anodes and cell walls due to convection in the bath and metal. In addition, the major heat generation occurs in the bath due to the voltage drops there, and the bulk of the Energy Imbalance in Eq. [2] therefore impacts on the bath directly. The anode and cathode heat generation contributions to the imbalance are much smaller, and any imbalances there are also communicated rapidly by convection to the liquid bath or metal from the solid anodes and cathode, respectively. The result is that the liquid bath itself is the focal point for energy imbalance in the cell, including those due to amperage changes.

As a first approximation, therefore, for the initial hours after the imbalance appears, the cell energy imbalance can be considered to report in the liquid bath with which the internal cell conductors (anode and cathode) are in intimate thermal contact:

$$d(M \cdot C_p \cdot T)\text{cell}/\text{d}t = d(M \cdot C_p \cdot T)\text{bath}/\text{d}t, \quad [3]$$

This approximation will be useful for a period of time not much longer than the first-order time constants of the anode and wall systems which are the fastest responding components of the cell heat loss. The wall can be considered as a simple slab (see Figure 1) which has a time constant dependent on the magnitude of step change in heat flow from either the bath or from the potshell where external regulation of the heat loss is being engineered. Work by Stewart[11] has allowed derivation of an expression for the thermal time constant for such a slab

$$\tau = (4/\pi^2)(L^2 \rho C_p/k)\, Ln(4/\pi\lambda), \quad [4]$$

where $(1 - \lambda) = Q_{\text{walls}}/h(T_{\text{bath}} - T_L)$ is the fractional reduction in the heat flux from the external wall with symbols as defined in Figure 1.

If the heat loss Q_{walls} is reduced by 60 pct due to a new insulating technology, then

$$\lambda = 0.6, \quad \text{and} \quad \tau = (3/\pi^2)(L^2 \rho C_p/k). \quad [5]$$

Based on Eq. [5] the time constant for the walls can be computed for a 0.2 m wall, including frozen ledge, to be ~2 hours, with an uncertainty of up to 1 hour dependent on frozen ledge thickness.[12] After this time, the reduction in the temperatures of the solid materials in the cell walls will act to reduce the heat losses there, creating a progressively greater error in Eqs. [1] and [2] over time.

Similarly, the heat loss through the anodes is subject to a time constant due to conduction vertically through the anodes, although the parallel heat flow paths of anode rod conduction and crust conduction/convection around the anodes make the estimation of this 'top heat loss' time constant more difficult and uncertain than for a simple slab.

What is known from aluminum smelter operating practice (anode covering operation) is that a reduction in the level of cover on the top of anodes can reduce the anode temperature at the level of the bath surface from 'red heat' or 873 K (600 °C), to under 773 K (500 °C) (black carbon appearance) within 20 to 30 minutes.[13] This indicates that the time constant for heat flow through the anodes is at least the same order of magnitude as the time constant for the walls.

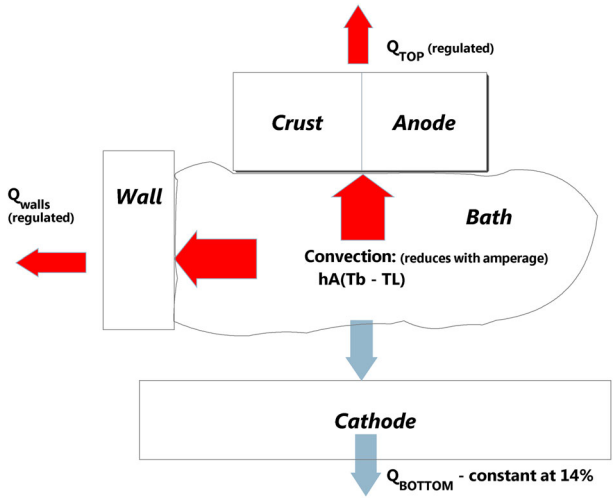

Fig. 1—Lumped heat capacity and slab model for dynamic response of bath.

For expediency here, therefore, and in deference to the other uncertainties, it will be assumed that the time constant for relaxation of the top heat loss due to reduced cell duct draft is also 2 hours, as for the walls of the cell.

Contributions in the first hours of the global heat balance from other cell components such as the metal pad are not quantified yet and could reduce to a degree the severity of the impact of the energy imbalance in the bath, computed in this work. The simulations given here can therefore be viewed by smelter management as conservative (= worst case). These other cell component contributions will be assessed in a more detailed dynamic simulation of the thermo-electric balance, which is outside the scope of the present study.

3. *Local energy imbalances causing freeze/melt of bath*

The second fundamental dynamic involves the local energy imbalances at the cooling solid interfaces, where freezing of bath can occur onto both the walls and the anodes—which are the surfaces in continuous contact with the liquid bath.

$$h_A(T_{bath}-T_L)_{walls+anodes} + \Delta H_{fusion} \times dM_{freeze}/dt = Q_{walls} + Q_{anodes}, \quad [6]$$

This equation applies exactly if the wall and anode flows from the freeze interface itself, into the sidewalls and anodes are able to be computed. However, these interfacial conductive heat flows are not known without detailed dynamic simulation of the interface behavior. The assumption made here is that at zero time, the conductive heat flows away from the freeze interfaces are equal to the steady-state heat losses through the wall and anodes, respectively—a steady state exists at time $t = 0$.

Along with the newly created imbalance between convective and conductive heat fluxes at these freeze interfaces in Eq. [6], the total rate of freezing of the bath depends also on how much surface area of sidewall and of anode is available for the bath to freeze onto. Here the full liquid height (including metal height) and the full anode table of the cell are available for the bath to freeze onto. This geometric situation could be varied, and especially depending on operational liquid height strategies prior to amperage reduction—for example, reducing the metal height or reducing the anode immersion, to reduce the surface area for heat loss and freezing.

An expression is also needed to determine the heat flow into the anodes themselves, as a fraction of the total top heat loss. In the present study, the heat loss through the anodes in Figure 1 is assumed to be 60 pct of the total top loss, based on steady-state thermo-electric simulations,[2] where values between 57.4 and 61.7 pct were obtained depending on anode immersion depth, and anode cover level. Total top heat loss has also been computed in these simulations and was found to be in the range from 46.7 to 52.5 pct of the cell heat loss depending on the depth and quality of anode cover applied. Here we use a value of 48 pct, since this also corresponds most closely with more detailed measurements and modeling of the top heat loss in a previous study.[14]

Both the wall and anode convective heat flows from the bath on the left-hand side of Eq. [6] are reduced as the bath superheat reduces and freezing occurs. These reduced heat flows from the bath 'buffer' the Global energy imbalance on the cell in Eq. [2], which then become

$$\Delta Energy_t = \Delta Energy_o - [Q_{walls} + Q_{anodes} - h_A(T_{bath} - T_L)_{walls+anodes}] \quad [7]$$

Equation [7] is the dynamic which gives rise to the phenomenon of 'thermal arrest' of the bath temperature as it reduces toward the liquidus temperature, which is itself reducing over time. The total reduction in convective heat transfer out of the bath, and therefore the extent of arresting of the bath temperature drop, depends again on the total interfacial area of bath contacting the walls and anodes, as well as possibly other interfaces such as the crust and the bath/metal interface. These latter interfaces are not included in the buffering of the convective heat loss considered in Eq. [7] because it is considered unlikely that the bath surface will remain in contact with the crust due to loss of bath height during freezing. The effect of the metal interface is unknown. however, and this is also omitted from the present dynamic response analysis although its higher total heat capacity may become important at some later time if the bath temperature is allowed to reduce significantly below that of the metal [for example, from the 1193 K to 1203 K (920 °C to 930 °C)] level.

Bath freezing is assumed to occur mainly as cryolite, giving rise to a higher AlF_3 pct in the remaining liquid bath, and reducing its liquidus point. This latter reduction is not necessarily at the same rate as the bath temperature reduction which is controlled initially by the global energy imbalance on the cell.

4. *Dynamics of cell wall heat loss and top heat loss reduction*

The third major dynamic in this process is introduced by the flexible production technology itself. The technology considered here allows closely controlled reduction in the convective heat losses from the potshell encasing the side and end walls, and from the anode rods and cover by reduced draft, when the reduced amperage is first applied to the cell or potline.

These insulated cell boundaries decrease heat flow through the walls and anode materials over time. This means that the 'baseline' for the Energy Imbalance calculation in Eq. [1] is actually changing, as the demand of the cell internal interfaces for heat dissipation reduces. The reduced $Q_{required}$, therefore, affects the 'steady state' value of $\Delta Energy_o$ by reducing the side/end wall heat flow to approximately 40 pct of the initial sidewall heat extraction, combined with a reduction to 70 pct of the initial top heat loss (through reduced cell duct draft). These figures are used here as the baseline-operating state for the flexible production technology which is currently being installed.

$$Q_{required} = Q_{bottom} + Q_{walls} + Q_{top}, \quad [8]$$

where Q_{walls} and Q_{top} are now reduced according to the performance of the flexible production technology. The simplified model described in this paper is shown in Figure 1.

The originally calculated 14 pct of heat loss through the bottom of the cell and collector bars remains unchanged in the time scale of the initial computation (a number of hours but less than a day). The remainder of the cell heat loss is subject to the previously estimated first-order time constants, τ, for the insulation of the walls, with 60 pct insulation using the heat exchangers, along with the 30 pct insulation of the top heat loss through reduced duct draft:

$$Q_{\text{required,t}} = 0.14 \times Q_{\text{original}} + (0.4 \times Q_{\text{walls,o}} + 0.6 \times Q_{\text{walls,o}} \times \text{EXP}(-t/\tau) + (0.7 \times Q_{\text{top,o}} + 0.3 \times Q_{\text{top,o}} \times \text{EXP}(-t/\tau)). \quad [9]$$

Therefore, the instantaneous global energy imbalance reduces over time because ΔEnergy_o is lowered by the impact of reducing Q_{required} as shown in Eq. [10]:

$$\Delta\text{Energy}_t = \Delta\text{Energy}_o - (Q_{\text{original}} - Q_{\text{required,t}}) - [Q_{\text{walls,t}} + Q_{\text{anodes,t}} - h_A(T_{\text{bath}} - T_L)_{\text{walls+anodes}}] \quad [10]$$

This imbalance initially starts at the value calculated above in Eq. [1]. It then reduces quickly due to reduced convective heat transfer to the walls and anodes as bath superheat is reduced. But ΔEnergy_t also reduces more slowly as the heat flows through the walls, crust, and anodes are reduced in the hours immediately after the insulation is applied.

It is this dynamic energy imbalance, as calculated in Eq. [10] which leads to the continuing drain on the enthalpy of the bath, and the loss of bath temperature is computed in Eqs. [2] and [3].

5. *Bath mass and composition change*

Equation [6] above allows the mass of freezing bath, M_{freeze}, to be computed over time. Integration gives the reduction in liquid bath mass after the energy imbalance is applied to the cell.

The bath composition change occurs as a result of preferential freezing of the cryolite component of the bath according to the phase equilibria first described by Grjotheim *et al.* in their seminal text, Aluminum Electrolysis[15] and more recently in the context of energy imbalances.[16] In this latter paper, the feasible operating region with respect to temperature and excess aluminum fluoride concentration is also described in detail, and the rate of change of liquidus temperature as a function of aluminum fluoride concentration is computed.

From the above works, it is evident that the mass of excess aluminum fluoride present in the liquid bath is concentrated within a smaller and smaller mass of liquid bath, creating an increase of ΔAlF_3 pct in excess aluminum fluoride concentration over any time step Δt. This increase gives rise to a corresponding change in bath liquidus point, according to

$$T_L = T_L + dT_L/d_{\text{AlF}_3} \cdot \Delta\text{AlF}_3\,\text{pct}, \quad [11]$$

where $d\text{T}_L/\text{d}_{\text{AlF}_3}$ is computed from the equation of Rostum *et al.*[17] for bath liquidus temperature (K per pct AlF_3) and is computed in Table I below, in the range from 8 to 20 pct AlF_3, using a fixed calcium fluoride level of 4.5 wt pct and an alumina concentration of 2 wt pct, both of which are based on measurements over a period of time on these cells. Although the rate of change of liquidus point clearly increases as aluminum fluoride content increases, this complexity has been omitted from the calculation in Eq. [11] where an averaged rate of change of liquidus temperature is used, between the starting excess aluminum fluoride concentration and a much higher future value arrived at through integration of the ordinary differential equations over time. Non-linearity in the rate of decline of liquidus temperature in the simulations below is therefore only attributable to non-linearity in aluminum fluoride concentration evolution.

Table I. Rate of Change of Liquidus Temperature with Excess Aluminum Fluoride Concentration

XS AlF_3 pct	$d\text{T}_L/\text{d}_{\text{AlF}_3}$
8	−3.24
10	−4.33
12	−5.47
14	−6.64
16	−7.84
18	−9.07
20	−10.32

The mean rate of change of liquidus point between excess aluminum fluoride concentrations of 10 and 20 pct is −7.28 K/pct AlF_3, from the table.

Small amounts of calcium fluoride, alumina, and aluminum fluoride do appear in the frozen ledge and solidified on the bottom of the crust.[18] However, these concentrations of impurity components in the ledge are too small (less than 1 wt pct) to change either the mass balance in the remaining bath, or its liquidus temperature. The liquidus point reduction is, therefore, determined according to the increase in aluminum fluoride concentration in the bath as it segregates into the reducing mass of liquid bath, according to Eq. [11].

The main uncertainty in the calculation of reducing liquidus point of the bath in Eq. [11] concerns the alumina concentration, which one would expect to increase in a similar way to the aluminum fluoride concentration if the alumina concentration was mass balance controlled. However, many dynamic observations of alumina mixing[19] indicate strongly that the alumina concentration is actually energy balance controlled, with the concentration of dissolved alumina often reducing toward the anode effect concentration of 1 to 2 pct, as surplus sensible energy for dissolution of further alumina additions reduces at lower bath superheats.

Therefore, no increase (or decrease) in the alumina concentration is assumed in this initial model for the electrolyte composition and liquidus temperature. Undoubtedly, this is an area where comprehensive, experimental bath composition measurements are necessary to establish the behavior of the alumina concentration after such an amperage reduction, since lack of dissolution may result in cessation of operations

if it occurs simultaneously on enough cells in the potline. This experimental work is planned for 2015 to 2016.

III. AMPERAGE REDUCTION WITHOUT FLEXIBLE PRODUCTION TECHNOLOGY

Solving the energy balance when there is no insulation of the walls or the top of the cell simplifies the above problem significantly since Q_{required} remains fixed in Eqs. [8], and [9] is not required. Therefore, Q_{required} is identical to Q_{original} in Eq. [10] and the only buffering of the initially applied energy imbalance occurs due to reduced convection to the walls and anodes of the cell. The reduced convective heat dissipation to these surfaces is buffered by freezing of bath, but at the cost of lost liquid bath volume.

Figure 2 shows this simulation, using an explicit finite difference scheme with time step of 0.02 hour (72 seconds). A very rapid loss in bath temperature and liquidus point is observed in Figure 2 as the bath freezes in the cell cavity. The corresponding reduction in mass of liquid bath is shown in Figure 3. It is evident from Figure 2 that after a period of 1.5 hour the bath temperature is less than 1173 K (900 °C).

In Figure 2, the energy imbalance produces immediate reduction in bath temperature to near the liquidus point and then freezing takes place at the rate of the energy imbalance across the bath/freeze interfaces in the cell. Reduction in bath temperature thereafter continues at more or less the rate of liquidus point reduction, as dictated by the freezing of bath shown in Figure 3.

Even with this buffering mechanism, the time to decrease bath temperature to 1173 K (900 °C) is only 1.5 hour, at which time the liquid bath mass has reduced to below 2500 kg, which is equivalent to a remaining bath height of less than 10 cm. This level of bath is considered to be below the minimum level at which an industrial cell can sustain electrolysis, due to excessive current density on the anodes and reduced alumina dissolution power.

It is observed in Figure 2 that the loss of bath temperature is accelerating with time as the aluminum fluoride concentrates into a lower and lower total liquid bath mass. In fact, the simulation after 1.6 to 1.7 hour reaches a critical phase, since the bath is approaching the point at which there is almost no cryolite left in the liquid phase, and will cease to dissolve any alumina at all below about 1153 K (880 °C).

Clearly, such a severe reaction to the amperage reduction (a MW reduction of 443 kW per cell) is too much to sustain for more than approximately 0.5 hour, when the bath temperature is already reduced to 1213 K (940 °C).

The latter stages of this simulation present a conservative view of the impact of the amperage reduction on the cell. This is because it has been assumed in this 'No Insulation' Case that the heat loss continues from the walls and top of the cell at the same rate as during full potline amperage and heat dissipation. An alternative assumption would be a gradual reduction in heat loss from both the top and the side and end walls of the cell, as a result of freezing of significant thicknesses of bath ledge on these surfaces.

We have not allowed for such a gradual reduction in heat loss in this simulation, although freezing of bath is obviously allowed for and, as we will see in subsequent simulations, reduction in heat losses do have a pivotal effect on conditions in the liquid bath.

However, the time constant of both the top (anodes and crust) and the walls is in the order of 2 hours, not minutes and therefore any significant reduction in heat losses will not occur immediately. So, the simulation above may be conservative in its prediction of impact on the bath over 2 hours, but is not unrealistic in the 30 to 60 minutes after the amperage reduction.

IV. AMPERAGE REDUCTION WITH FLEXIBLE PRODUCTION TECHNOLOGY APPLIED

Unless the time of current reduction is only 30 minutes or less, the loss of 251 kW of heat input as computed in

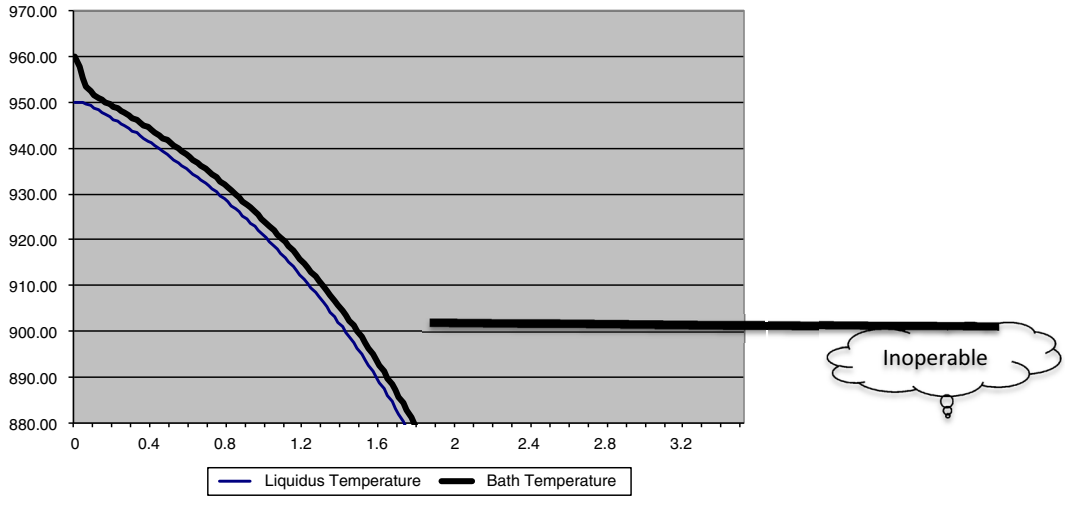

Fig. 2—Reduction in bath and liquidus temperatures (in °C) after reduction in amperage by 80 kA for case involving use of current smelting technology (no insulation of walls or top of cell).

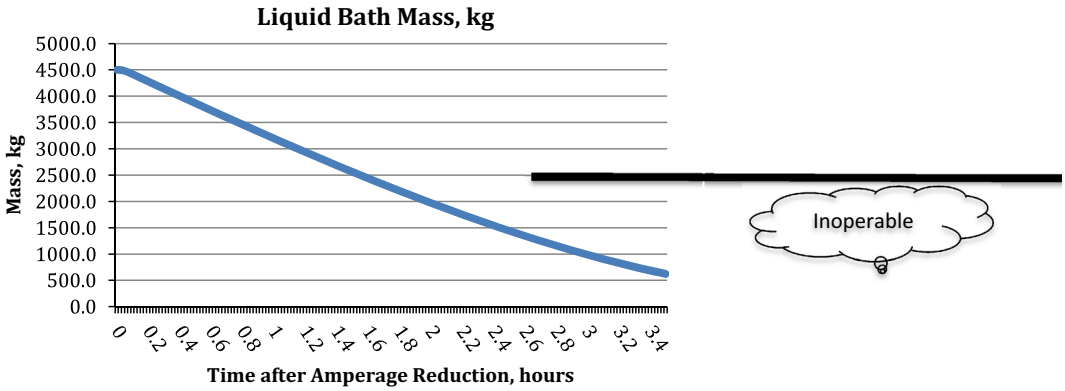

Fig. 3—Reduction in liquid bath mass after the amperage reduction in Fig. 1. No insulation case.

Section II–B for a cell with uncontrolled heat losses is clearly too large for sustained operation. For short time periods or small amperage reductions, an increased ACD strategy would provide extra, internally generated heat to reduce the imbalance as discussed by Stam and Schaafsma[5] in their work at Aldel in The Netherlands. In fact their radical solution at Aldel involved a reduction in ACD so that the anodes intermittently contacted the metal pad, giving rise to extra heat generation through back reaction without reduction in bath height.

Unfortunately, all attempts to compensate for such large energy imbalances through ACD change have been unsuccessful due to the other 'side effects' such as anode problems or cathode problems (dropping of crust pieces) or crust deterioration itself. Some of these side effects only emerge after several months, but in all cases, the practice of ACD change has been discontinued. It is also true that in the case of the 80 kA reduction considered here, or similarly large reductions on other cells, too much additional ACD would be required and bath levels would then be insufficient. From these considerations and the simulation in Section III, the present Case Study is therefore not a practical operating option without Flexible Production Technology.

The heat losses from the walls and from the top of the cell are substantially reduced in this technology,[2] in order to reduce the heat imbalance after the amperage reduction. This heat loss turndown mechanism allows 60 to 70 pct reduction in side and endwall heat loss, plus a reduction in top heat loss due to cell draft reduction of 30 to 40 pct.

In these flexible production scenarios, the simulation must use Eqs. [8], [9], and [10] as derived in Section II–B in order to determine the reduced global energy imbalance which applies over time.

A. *Base Case Heat Loss Reduction*

The wall heat exchanger technology is assumed here to reduce heat loss by 60 pct on the total side/end wall structure of the cell. This is a question of design of course—in fact, the sidewalls are 80 pct covered by the heat exchangers and there are provisions for the end walls to be flexibly insulated as well. So, a reduction of 60 to 70 pct is easily achievable, with some heat still being extracted from the regions of the walls with the highest incident heat flux from the bath and metal.

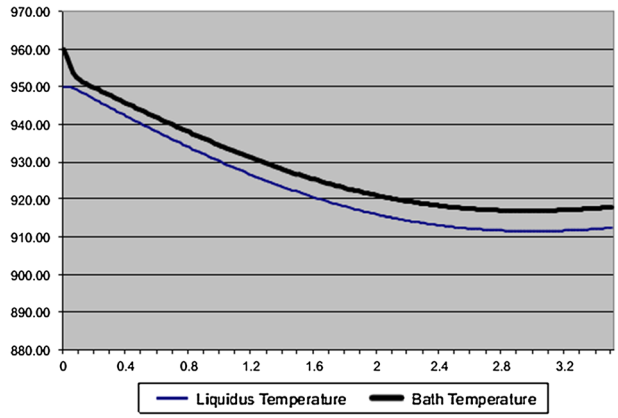

Fig. 4—Bath and liquidus temperature reduction for the base case in heat loss reduction: 60 pct wall heat loss reduction and 30 pct top heat loss reduction.

In addition, a 30 pct reduction in the top heat loss due to adjustment of potline draft is assumed, based on earlier computational and experimental studies.[14] Both the wall and top heat loss reductions are assumed to take place according to Eq. [9] with the first-order time constant set at 2 hours.

The result of this simulation is shown below in Figure 4. The effect of a reduced global cell heat imbalance, due to the progressively larger effect of the insulation of the walls and top of the cell over time, plus the effect of reduced local heat imbalances on bath freezing rate, combines together to produce a completely different result for the cell, from that shown earlier in Figure 2.

The initial reduction in bath temperature is similar to that observed in the un-insulated case in Figure 2. However, after the first 10 to 20 minutes, the reduction in temperature is much slower, and bottoms out at 1203 K (930 °C) after 3 hours, with more than 2950 kg liquid bath still available as shown in Figure 5 below.

Even more importantly the bath superheat recovers to 5 K (5 °C) where alumina dissolution is possible, and the cell slowly begins to recover in temperature and liquid mass after 3.5 hours. Given the assumptions made in arriving at this result—especially in terms of heat loss

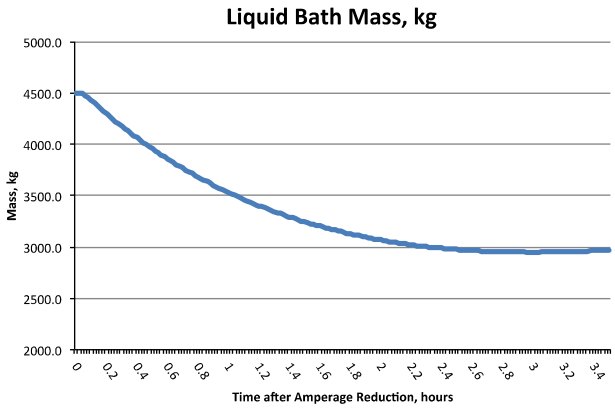

Fig. 5—Reduction in liquid bath mass for base case in heat loss reduction.

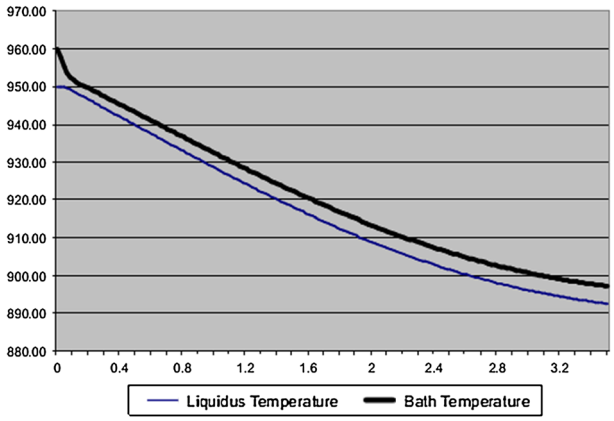

Fig. 6—Bath and liquidus temperature reduction for the case of 60 pct wall heat loss reduction and 10 pct top heat loss reduction.

from the walls of the cell—it is now important to understand the sensitivity of the cell response to varying levels of heat loss from the walls and the top of the cell.

B. *Lower Heat Loss Reduction from the Top of the Cell*

In Figure 6, the effect of a lower heat loss reduction from the top of the cell is investigated. Instead of the 30 pct reduction in the base case simulation, a reduction of only 10 pct in top heat loss is made here, with the same cell wall insulation applied as in the Base Case (Figures 4 and 5).

There is a dramatic difference in the effectiveness of the buffering in thermal impact for the cell in this case. Now after 3.0 hours the bath temperature is still reducing and is below 1173 K (900 °C) which is inoperable in terms of smelter cell operations. After 3.5 hours the bath temperature is still reducing, and Figure 7 shows that the liquid bath mass reduction is significantly higher than in the base case and the bath level will be reduced to only 10 cm.

In fact, Figure 7 is an under-estimate of the liquid bath mass reduction in this case, because (as in the first, uncontrolled heat loss case) the bath temperature has reduced to the level where massive freezing of bath could

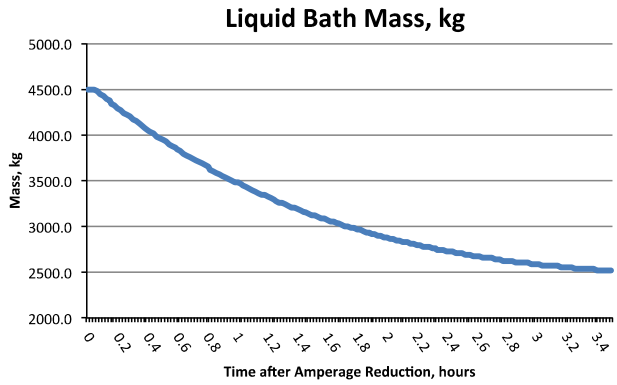

Fig. 7—Liquid bath mass reduction in the case of 60 pct wall heat loss reduction and 10 pct top heat loss reduction.

occur on the anodes, or elsewhere. No bulk liquid freezing mechanism is included in the model developed in Section II, because it leads to the breakdown of the lumped heat capacity assumption for the bath, and loss of the geometric contact areas assumed with the walls and anodes of the cell. In fact, these very low temperatures and low bath heights could easily be accompanied by loss of electrical continuity between the anodes and the bath on some cells in a potline.

In this particular case, therefore, we can envisage a longer period of 1.0 to 1.5 hour at the reduced amperage of 160 kA, without serious consequences for the cell. However, there is no chance that this situation is sustainable in terms of amperage turndown. Within 3 hours, the cell becomes inoperable.

Clearly, more thermal regulation of the top of the cell is required in order for this case study to be viable.

C. *Lower Heat Loss Reduction from the Walls of the Cell: 50 Pct Reduction Only*

In this case, the wall heat loss reduction is envisaged to be less effective—a 50 pct reduction instead of 60 pct reduction in wall heat loss, but with the same time constant of two hours and the same top heat loss reduction. Figure 8 shows the bath and liquidus temperature response to the amperage reduction in this case.

The response of the cell in this case is similar to that in the last case involving lower top heat loss reduction. In Figure 8, the temperature reaches 1173 K (900 °C) after 3.5 hours and is still decreasing, along with the liquidus temperature. Evidently, a 10 pct lower level of insulation in wall heat loss has caused the response of the bath to become inoperable, as it did in the previous case, after about 2 hours. Liquid bath mass reduction is also similar to the last case.

This simulation shows the high sensitivity to thermal regulation which the cell exhibits, in the case of the large amperage reduction required here.

D. *Higher Heat Loss Reduction from the Walls: 70 Pct Reduction in Wall Heat Loss*

A 10 pct higher degree of wall insulation is applied in this case, for comparison with the base case 60 pct. In Figure 9, the bath response of the cell is shown.

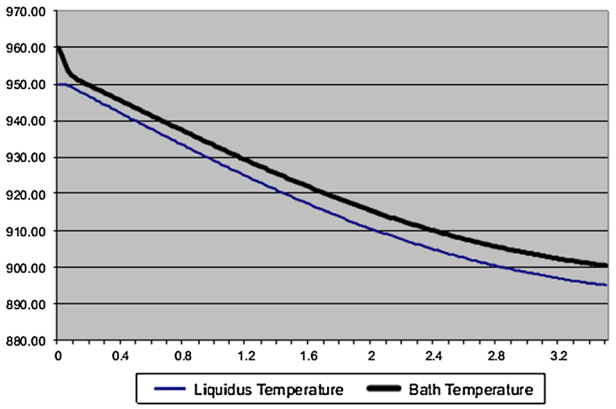

Fig. 8—Reduction in bath and liquidus temperature in the case of a 50 pct wall heat loss reduction and 30 pct top heat loss reduction.

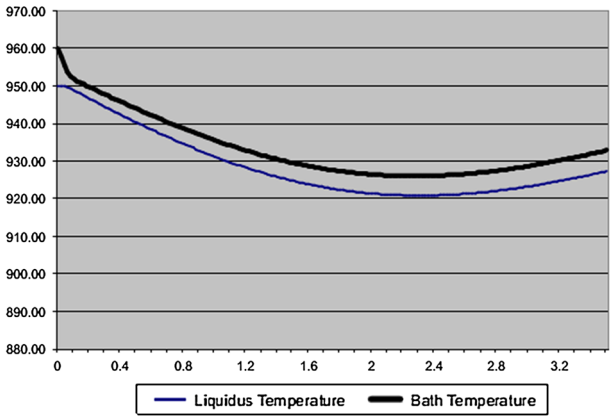

Fig. 9—Reduction in bath and liquidus temperature due to a 70 pct wall heat loss reduction and 30 pct top heat loss reduction.

Now it is clear that after 2 hours—the time constant used to describe the thermal response of the walls and the top of the cell—the recovery of bath temperature, composition, and bath mass (Figure 10) from the effects of amperage reduction is rapid. Results after 3.2 hours show a bath temperature above 1203 K (930 °C) again, a bath superheat above 5 K (5 °C) and a bath mass which is 3400 kg.

At 2.3 hours after the amperage reduction, a minimum temperature of 1199 K (926 °C) is predicted. The highest excess aluminum fluoride is also recorded at this time and is 14 pct, which is significantly better than the 15.3 pct concentration in the base case. This bath condition is not one we would want to sustain for an extended period due to poor alumina dissolution and the risk of freezing of sludge on the cathode of the cell. However, as a transient for 1 to 2 hours before recovery to normal bath conditions, it is quite feasible.

Many questions remain unanswered about this last observation of course…What if there is a whole potline of cells at 1193 K to 1203 K (920 °C to 930 °C) at the same time? What is the effect of setting anodes in (many) such cells—or should anode setting be delayed until the recovery of the bath to above a certain temperature? Can anode effects be terminated when they are occurring on many of these cells at once?

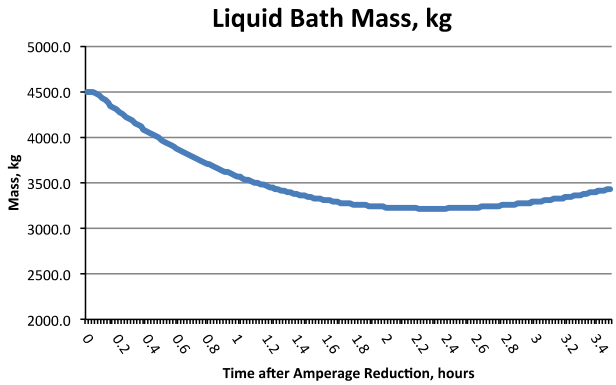

Fig. 10—The reduction in liquid bath mass due to the 70 pct wall heat loss reduction and 30 pct top heat loss reduction.

These questions cannot be answered on the basis of the simple thermal model presented here, or indeed without comprehensive experimentation on the transient behavior of alumina feeding and dissolution in this reduced heat dissipation situation.

V. DISCUSSION

The foregoing analysis indicates that on the most basic criterion of bath temperature, superheat, and liquid bath mass maintenance, there is reasonable evidence that the Flexible Production Technology proposed can control amperage reduction situations of the magnitude in this case study.

However, there are two issues which have been raised in this analysis:

- The sensitivity of the cell response to the regulation of heat loss, necessitating precise control of heat loss using the patented heat exchanger technology.
- The limitations of the present simple model for assessing the dynamic response of the cell.

A. *Sensitivity of Cell Response to Regulation of Heat Loss*

Evidently, the operating point of 160 kA and 3.235 V cell voltage could be sustainable under the insulated conditions produced by the flexible production technology, if other factors such as cell operations and alumina feeding at low superheat can be managed. This is a reduction in power input of 46 pct which would normally require the stopping of whole potlines.

However, relatively small changes in wall or top heat loss regulation completely changed the operability of the cell simulated, following the reduction in amperage. Furthermore, the modeling to date is not precise enough to ensure a reliable heat extraction target for the heat exchanger technology. For example, it is possible that variations in the initial state of the bath in different cells in the potline are sufficient to cause a selected insulating level to be inappropriate for maintaining the bath in all cells at operable electrolysis conditions.

The observations here imply that finely tuned real-time control of the thermal insulation level of the walls will be required for this technology and that individual cell adjustments in thermal regulation are important.

B. *Limitations of the Present Model*

Section II–B of this paper details the computational assumptions employed here. However, an over-riding assumption of a lumped heat capacity model is that there is a well mixed region for the material constituting the heat capacity. In fact, modern smelting cells are in excess of 13 to 14 m long, and each end of such a cell is not in good thermal or compositional connection with the other. The ends and corners of the cell are most at risk of not being represented by the present model. It is already known that setting of anodes in the corner positions in any cell is most difficult for purely thermal reasons. This corner position sensitivity is likely to be even more severe in reduced amperage situations. A geometrically representative model for the corners of the cell will be essential, as part of the next refinement in the investigation.

The second issue relates to the degree of buffering by convective heat dissipation from the bath to the interfaces in contact with it. In the present paper, we have made a reasonable but far reaching assumption about the interfacial area for convection between the bath, and the walls and immersed anodes. No computation of the effect of changes in bath height, or the effect of the metal convection back into the bath has been attempted. A greater extent of convective heat transfer area from the bath will cause a greater initial thermal arrest in the bath temperature, but a faster reduction in liquid bath mass and ultimately a more rapid decline of the bath temperature. Conversely, a smaller interfacial contact area for the bath will give rise to less convection and freezing, leading to more reduction in temperature and superheat in particular, but less freezing of bath.

This latter convection-related characteristic will affect the degree of bath temperature reduction and the magnitude of bath superheat, but not the overall energy imbalance or the time for recovery of this energy imbalance in the bath which is determined mainly by the time constant and degree of insulation of the walls and top of the cell as demonstrated in Section III.

The last limitation of the model concerns the role of alumina dissolution in stabilizing or destabilizing the electrolysis process under the conditions described here. There is a small amount of laboratory and experiential smelter knowledge concerning the ability of cells to sustain alumina dissolution in cryolite-based baths below 1203 K (930 °C). However, there is no predictive information concerning the effect of low temperatures and superheat on the dissolved alumina concentration itself—especially under reduced amperage conditions. Maintaining an alumina concentration of 2 wt pct or more is crucial to the viability of the flexible production technology discussed in this paper, since all cells in a potline will need to be operable in terms of electrolysis and not just liquid bath volume, for a sustainable potline operation.

Much more research is needed in both fundamental alumina dissolution kinetics at low superheat, and in the practical issues of controlling the feed rate to avoid anode effects and concentration gradients in the industrial cells. This is an objective of the current research program.

VI. CONCLUSIONS

The results of the simulations reported here provide strong evidence that the heat loss regulation technology is a feasible mechanism for recovering and sustaining a viable energy balance at two-thirds of the normal potline amperage. Although much confirmatory work remains, it is evident that 60 to 70 pct reduction in the wall heat loss and 30 pct reduction in the top heat loss are likely to be a good target for the regulation of heat losses.

The reduction in cell power usage computed in this paper is 46 pct, indicating that the smelter could shed more than 370 MW of its total load without reducing the number of cells in circuit, and remain operable, at a DC power efficiency of 10.5 kWh/kg, compared to its normal efficiency of 12.7 kWh/kg. This result, and its sustainability, opens the way for flexible production of aluminum in a way that releases electricity network constraints in the way that was described in the Introduction to this paper.

The sensitivity with respect to the level of heat loss regulation of the cell responses simulated here indicates that individual cell heat loss regulation will be needed, and this is already incorporated in the heat exchanger design.

The assumptions and observations in Section II and IV also provide guidance about the next stages of modeling and smelter measurements for implementation of the flexible production technology:

- Intensive measurement and validation of the simulated bath temperature, liquidus point, and bath mass during controlled amperage reductions are important to confirm the work reported here.
- Intensive measurement of the bath composition, and particularly the alumina concentration during the period before and after amperage reduction—for at least 4 hours and possibly longer.
- A coarse geometric model of the cell with more lumped heat capacities, allowing detailed simulation of the three main bath dynamics—global energy imbalance, local energy imbalances, and wall and top heat loss reduction—is needed. The effects of the metal pad and the cathode should be included in this new model, along with more detailed thermal relaxation of the walls, crust, and anodes.

ACKNOWLEDGMENTS

The authors are grateful to the Ministry of Business, Innovation and Employment (MBIE) in New Zealand for funding this research. We also wish to thank Florence Taylor for her artwork and management of the manuscript.

REFERENCES

1. J. Petrovic and G. Thomas: "Reaction of Aluminum with Water to Produce Hydrogen", US DOE Report, 2008.
2. M.P. Taylor, R. Etzion, P. Lavoie, and J. Tang: *Metall. Mater. Trans. E*, 2014, vol. 1E, pp. 292–302.
3. P. Lavoie, S. Namboothiri, M. Dorreen, J.J.J. Chen, D.P. Zeigler, and M.P. Taylor: in *TMS Light Metals*, 2011, pp. 369–74.
4. L.J. Pinheiro Leal Nunes, A. Vianna da Silva, and L.F. Gomes Soutinho: in *Light Metals*, 1998.
5. M.A. Stam and J. Schaafsma: *Proc. 9th Aust. Al. Smelting Tech. Conf.*, Terrigal, NSW, Australia, 2007.
6. http://www.bhpbilliton.com/home/investors/news/Pages/Articles/South%20African%20Power%20Reduction%20Impact%20On%20BHP%20Billiton%20Aluminium.aspx. Accessed 12 Feb 2015.
7. M.P. Taylor, J.J.J. Chen, M. Farid, and R.J. Wallace: US Patent 7,901,617 B2, 2011.
8. M.P. Taylor, J.J.J. Chen, M. Farid, and R.J. Wallace: US Patent 8,778,257 B2, 2014.
9. Post Graduate Certificate in Light Metals Reduction Technology, University of Auckland, held at Essen and Hamburg, Germany, May 2012.
10. L. Cassayre, P. Palau, P. Chamelot, and L. Massot: *J. Chem. Eng. Data*, 2010, vol. 55, pp. 4549–60.
11. D.B. Stewart: *Build. Environ.*, 1981, vol. 16 (2), pp. 87–91.
12. M.P. Taylor, W.D. Zhang, V. Willis, and S. Schmid: *Chem. Eng. Res. Des. Trans. I. Chem. E*, 1996, vol. 74, p. 913.
13. E.W. Andrews, M.P. Taylor, G.L. Johnson, and I. Coad: in *Light Metals 2005*, H. Kvande, ed., Minerals, Metals & Materials Society, San Francisco, CA, 2005, pp. 357–62.
14. H. Abbas, M.P. Taylor, M. Farid, and J.J.J. Chen: in *Light Metals 2009*, G. Bearne, ed., Minerals, Metals and Materials Society, San Francisco, CA, 2009, pp. 551–56.
15. K. Grjotheim, C. Krohn, M. Malinovsky, K. Matiaasovsky, and J. Thonstad: *Aluminium Electrolysis: The Chemistry of the Hall–Heroult Process*, 1977, ISBN-13:978-3870171292.
16. M.P. Taylor: *Proceedings of the 5th International Conference on Molten Slags, Fluxes and Salts, ISS-AIME*, Sydney, Australia, 1997, pp. 659–74.
17. A. Rostum, A. Solheim, and A. Sterten: in *TMS Light Metals*, 1990, p. 311.
18. Q. Zhang, M.P. Taylor, J.J.J. Chen, D. Cotton, T. Groutzo, and X. Yang: in *TMS Light Metals*, 2013, pp. 675–80.
19. B.J. Welch, J.J.J. Chen, W.D. Zhang, J.M. Purdie, and M.P. Taylor: *Mater. Sci. Forum*, 1991, vol. 73–75, pp. 779–87, Trans Tech Publications, Switzerland.